ARTICLE INFO
Article ID: 10-10-03-0024
© 2026 The Authors
doi:10.4271/10-10-03-0024

Impact of Network-Induced Delays on Autonomous Vehicle Steering Stability

Jialin Li,[1] Jianwei Lu,[3] Heng Wei,[3] and Di Ao[2]

[1]Nanjing University of Industry Technology, School of Transportation Engineering, China
[2]Institute of Facility Agriculture, Guangdong Academy of Agricultural Sciences, China
[3]Hefei University of Technology, School of Automotive and Transportation Engineering, China

Abstract

This article presents a cross-layer framework that integrates realistic vehicle-to-network-to-vehicle (V2N2V) delay characterization with a rigorous stability analysis of automated vehicle steering control. Both constant and network-induced time-varying delays modeled via deterministic bounds are addressed. For constant delays, delay-independent stability regions within the controller gain space are analytically derived. For time-varying delays with stochastic network origins, modeled using deterministic bounds, a refined Lyapunov–Krasovskii functional (LKF) incorporating augmented single- and double-integral terms is constructed. To establish delay-dependent linear matrix inequality (LMI) conditions, a reciprocally convex combination approach is employed to handle the delay interval partitioning, and the second-order Bessel–Legendre inequality is applied to tighten the integral quadratic bounds. The resulting LMI conditions explicitly capture the coupled effects of delay magnitude, delay variation rate, and control gains on closed-loop stability. Simulations of a lane-keeping scenario confirm that the predicted stability boundaries accurately match the closed-loop system behavior. Notably, incorporating a realistic time-varying V2N2V delay profile into the controller design reduces the lateral-state root-mean-square error (RMSE) by over 54% and decreases the settling time by a factor of 10 compared to designs relying on an average-delay assumption. However, high packet loss rates are shown to still induce residual oscillations due to information scarcity. Ultimately, these results elucidate delay-induced instability mechanisms and provide practical guidelines for designing delay-robust steering controllers for connected and automated vehicles.

History

Received: 22 Jan 2026
Revised: 08 May 2026
Accepted: 02 Jun 2026
e-Available: 25 Jun 2026

Keywords

Autonomous vehicle, Steering control, Stability analysis, Delay, V2N2V

Citation

Li, J., Lu, J., Wei, H., and Ao, D., “Impact of Network-Induced Delays on Autonomous Vehicle Steering Stability,” *SAE Int. J. Veh. Dyn., Stab., and NVH* 10(3):515-533, 2026, doi:10.4271/10-10-03-0024.

ISSN: 2380-2162
e-ISSN: 2380-2170

1. Introduction

Steering control [1] is a vital component of automated driving systems, directly affecting vehicle stability, maneuverability [2, 3], and safety in typical driving tasks such as lane-keeping [4] and path-following [5–7]. The emergence of connected and automated vehicles (CAVs) has enabled cooperative functionalities, such as platooning [8], cooperative lane-changing [9, 10], and cloud-based path planning [11], through V2N2V communication. However, such networked control architectures introduce end-to-end (E2E) communication delays ranging from constant delays to network-induced time-varying delays, which originate from stochastic communication effects but are modeled here using deterministic bounds and are often subject to packet loss, all of which pose significant challenges to closed-loop stability [12–15]. Specifically, communication delays introduce phase lag and effectively reduce the damping of the closed-loop system, which may lead to oscillatory responses, degraded tracking accuracy, and even instability in extreme cases. Time-varying delays further exacerbate this issue by inducing parameter uncertainties and dynamic coupling effects, making the stability region highly sensitive to both delay magnitude and its rate of variation [16–18].

Unlike mechanical or filtering delays [19–22] that remain relatively constant, V2N2V communication delays exhibit high variability due to congestion, handover, and wireless channel fluctuations. Existing steering controllers, whether model predictive control [15, 23, 24], or nonlinear control regimes [25–27], typically assume instantaneous or delay-free actuation [28], which is unrealistic in networked settings. Although some studies explicitly model delayed states [29], the majority are limited to constant delay assumptions, failing to capture the dynamic and stochastic features of network-induced latency. As a consequence, existing methods may significantly overestimate the stability margin or fail to predict oscillatory behaviors under realistic network conditions [30], especially when delay variations interact with vehicle lateral dynamics.

For constant delays, classical delay differential equation methods [31] and semi-discretization techniques [6, 32] can generate stability charts, but they suffer from two key limitations. They cannot determine delay-independent stability regions where the system remains stable regardless of delay magnitude [33, 34], and they require exhaustive numerical sweeps to identify critical delay thresholds for specific parameter combinations [35]. To overcome these limitations, this article combines Lyapunov–Krasovskii functional (LKFs) [36], which establishes delay-independent regions, with Routh–Hurwitz ($\mathcal{R}-\mathcal{H}$) criteria and marginal stability analysis to analytically derive critical delay bounds in the delay-dependent region [25, 37]. However, these approaches still exhibit considerable conservatism due to the use of conventional Lyapunov functionals and coarse bounding techniques, which limit their ability to accurately characterize the true stability boundary.

For network-induced time-varying delays, the challenge intensifies as network-induced delays fluctuate randomly within stochastic intervals and are subject to packet drops [38, 39]. While dropped packets can be modeled as extreme delay cases, practical V2N2V systems employ retransmission or zero-order-hold (ZOH) strategies that bound the effective delay [40]. Under such mechanisms, the system experiences time-varying delays with stochastic variation rates, which depend on network quality metrics such as packet loss [41, 42]. To address this, we employ refined integral inequality techniques in conjunction with LMI formulations to derive stability conditions that explicitly account for delay upper bounds and variation rates. This approach not only ensures theoretical rigor but also provides practical guidelines. High-fidelity V2N2V simulations validate these thresholds and demonstrate graceful performance degradation under varying network conditions [43]. The coupling between delay magnitude and its variation rate introduces an additional degree of complexity, as rapid delay variations can destabilize the system even when the average delay remains moderate.

Based on the above discussions, this article conducts a comprehensive stability analysis of networked vehicle steering control under constant and time-varying communication delays. The key contributions are summarized as follows:

- A LKF analysis establishes a delay-independent stability region, providing a robust design space irrespective of delay magnitude. Outside this region, a $\mathcal{R}-\mathcal{H}$ analysis shows that the critical delay threshold decays with the control gains: aggressive gains tolerate shorter delays, whereas conservative gains preserve stability under longer delays. These properties enable adaptive gain scheduling based on real-time delay measurements.
- An enhanced LKF incorporating augmented single- and double-integral terms is constructed. The reciprocally convex combination is then used to handle the time-varying delay partition, and the second-order Bessel–Legendre inequality is applied to tighten the integral quadratic bounds, yielding less conservative delay-dependent LMI stability conditions. These conditions explicitly capture the coupled effects of delay upper bounds and delay rate variations on the stability region. The analysis shows that increasing delay variability significantly shrinks the admissible stability margin.
- Simulations demonstrate that incorporating the measured time-varying delay profile, rather than relying on a simple average-delay assumption, substantially reduces steering oscillations and shortens settling time under realistic V2N2V communication conditions. From an engineering perspective, this result indicates that average delay–

based controller tuning can lead to insufficient robustness when delay fluctuations and packet loss events are significant. The analysis therefore provides practical guidance for implementing delay-aware control strategies and establishes minimum communication-reliability requirements for stable and smooth steering performance.

The remainder of this article is organized as follows. Section 2 explains the problem formulation and the mathematical modeling of the steering control system with delays. Section 3 derives the delay-independent and delay-dependent regions and discusses their implications, and solves LMI-based stability regions for network-induced time-varying delays. Section 4 validates the proposed methods through numerical simulations and discusses the results. Finally, Section 5 concludes the article and outlines potential directions for future research.

2. System Modeling and Steering Control Design

2.1. Closed-Loop Time Delay System

In this study, the lateral dynamics of the vehicle are described using a planar single-track (bicycle) model, as depicted in Figure 1. This model is widely adopted for capturing the dominant yaw and lateral motion characteristics of road vehicles while maintaining a compact representation suitable for control-oriented analysis.

The vehicle motion is described with respect to a ground-fixed (X, Y) inertial frame, whose orientation is defined by the yaw angle ψ. A vehicle-fixed (x, y) coordinate system is attached to the center of gravity (CoG) G, where the longitudinal and lateral velocities are denoted by V_x and V_y, respectively. The lateral dynamic states considered in this work are the yaw rate γ and the sideslip angle β, while the front-wheel steering angle δ serves as the control input.

FIGURE 1 Representation of single-track dynamics model.

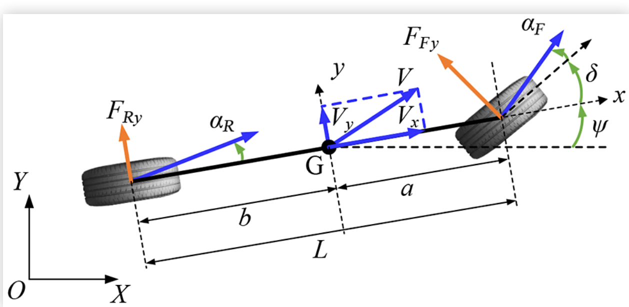

TABLE 1 Vehicle parameters (corresponds to Figure 1).

Symbol (unit)	Description	Value
m (kg)	The total mass of the vehicle	1270
I_z (kg · m^2)	Yaw moment inertia	1536.7
L (m)	Length of wheelbase	2.91
C_F (N/rad)	Front cornering stiffness	–107,610
C_R (N/rad)	Rear cornering stiffness	–74,520
a (m)	The distance from CoG to front axle	1.015
b (m)	The distance from CoG to rear axle	1.895
V_x (km/h)	The velocity of the vehicle	80

The vehicle has a total mass m and a yaw moment of inertia I_z. The distances from the CoG to the front and rear axles are denoted by a and b, respectively, yielding a wheelbase length $L = a + b$. All physical parameters used in the model are summarized in Table 1.

Under the small-angle assumption and neglecting longitudinal dynamics, the lateral motion of the vehicle is governed by

$$\begin{cases} mV_x\left(\dot{\beta}+\gamma\right) = F_{Fy}\cos\delta + F_{Ry} \\ I_z\dot{\gamma} = aF_{Fy}\cos\delta - bF_{Ry} \end{cases} \tag{1}$$

where F_{Fy} and F_{Ry} represent the lateral tire forces generated at the front and rear axles, respectively.

The lateral tire forces are modeled using a linear tire model (2) based on the slip angles α_F and α_R of the front and rear wheels, respectively. This linear approximation is valid under small slip angle conditions, which are commonly satisfied in normal driving scenarios such as lane-keeping and path-following. Moreover, since the primary objective of this study is to analyze the impact of communication delays on closed-loop stability, the use of a linear tire model enables tractable analytical derivation while preserving the essential lateral dynamics of the vehicle. Specifically, the lateral forces are expressed as

$$\begin{cases} F_{Fy} = -C_F\alpha_F \\ F_{Ry} = -C_R\alpha_R \end{cases} \tag{2}$$

where C_F and C_R represent the front and rear tires' lateral stiffness.

From a kinematic perspective, the slip angle of the front and rear tires is defined as follows

$$\begin{cases} \alpha_F = \arctan\left(\beta + \dfrac{a\gamma}{V_x}\right) - \delta_d \\ \alpha_R = \arctan\left(\beta - \dfrac{b\gamma}{V_x}\right) \end{cases} \tag{3}$$

2.2. Network-Induced Delay Modeling in V2N2V Systems

A typical driving scenario (i.e., teleoperation driving) under the V2N2V architecture, as illustrated in Figure 2, the closed-loop control performance is fundamentally constrained by E2E latency. The system operates under a sequential process of uplink transmission (τ_{ul}), control computation (τ_p), downlink transmission (τ_{dl}), and vehicle actuation (τ_a). The total latency $\tau(t)$ is an aggregation of multiple stochastic components, each corresponding to a specific segment of the following data flow:

$$\tau(t) = \tau_{ul}(t) + \tau_p(t) + \tau_{dl}(t) + \tau_a(t) \tag{4}$$

The temporal variability of these delays, induced by wireless channel fluctuations, computational load dynamics, and network congestion, results in stochastic and time-varying E2E latency [44]. The statistical characteristics of the delay $\tau(t)$, including its probability density distribution and time-varying properties, are further analyzed and illustrated in Section 4.2 based on simulation results.

The impact of these delays is critically reflected in the information freshness at the controller, quantified by the Age of Information (AoI) [42, 44]. As depicted in the communication timeline of Figure 3(a), AoI is defined as the time elapsed since the generation of the most recently received valid uplink packet at the vehicle ($t_{P,m(n)}$) until its processing by the controller ($t_{C,n}$):

$$\Delta t_{age}(t_{C,n}) = t_{C,n} - t_{P,m(n)} \tag{5}$$

Figure 3(b) clearly shows the sawtooth pattern of AoI evolution: it increases linearly during periods of packet loss or delay and resets upon the successful reception of a fresh data packet. A key phenomenon observed is the non-sequential and merged perception of packets at the controller due to packet loss, where multiple transmitted packets (e.g., $m = 0$, $m = 3$, $m = 6$) may be effectively perceived as a single sampling event ($n = 0$). Under such packet loss conditions, the controller implements a zero-order hold strategy, maintaining the previous control command until a new packet arrives, thereby ensuring control signal continuity at the cost of increased information staleness.

2.3. Controller Design under Constant Delay

To establish a reference case and facilitate analytical tractability, the communication delay is first assumed to be constant and denoted by τ. Under this assumption, the steering command is generated via a linear state feedback law based on the delayed vehicle sideslip angle β and yaw rate γ, expressed as

$$\delta_d(t) = -k_p\beta(t-\tau) - k_d\gamma(t-\tau) \tag{6}$$

where k_p and k_d represent the feedback gains, respectively (hereafter referred to as state feedback control).

By substituting the control law into the linearized lateral vehicle dynamics, the closed-loop system can be formulated in a compact state-space representation as

$$\dot{x}(t) = \mathrm{A}x(t) + \mathrm{BK}x(t-\tau) \tag{7}$$

where the state vector is defined as $x(t) = [\beta(t), \gamma(t)]^T$ and the gain vector is given by $\mathbf{K} = [-k_p, -k_d]$.

$$\mathrm{A} = \begin{bmatrix} \dfrac{C_F + C_R}{mV_x} & \dfrac{aC_F - bC_R}{mV_x^2} - 1 \\ \dfrac{aC_F - bC_R}{I_z} & \dfrac{a^2C_F + b^2C_R}{I_zV_x} \end{bmatrix}, \quad \mathrm{B} = \begin{bmatrix} -\dfrac{C_F}{mV_x} \\ -\dfrac{aC_F}{I_z} \end{bmatrix} \tag{8}$$

FIGURE 2 Architecture of the proposed networked autonomous steering control system. The vehicle performs automated steering using an onboard sensing and actuation system, while the steering control algorithm is executed at a remote computation center through a V2N2V communication loop. No human operator is involved in the control process.

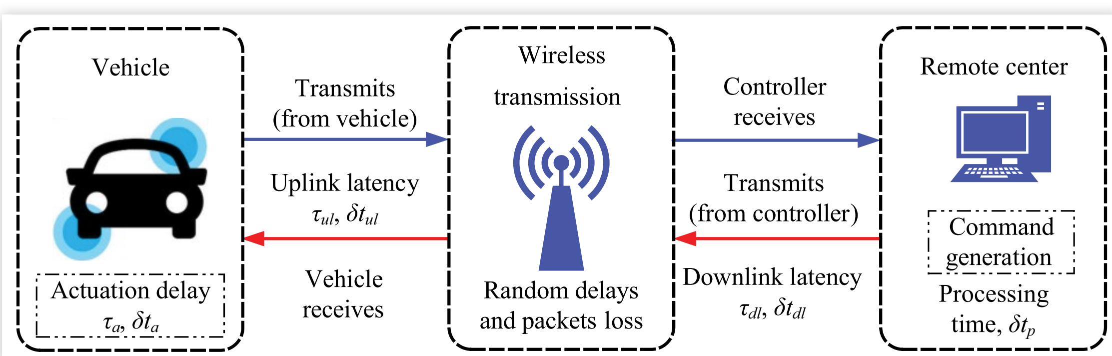

FIGURE 3 Time delay modeling and analysis.

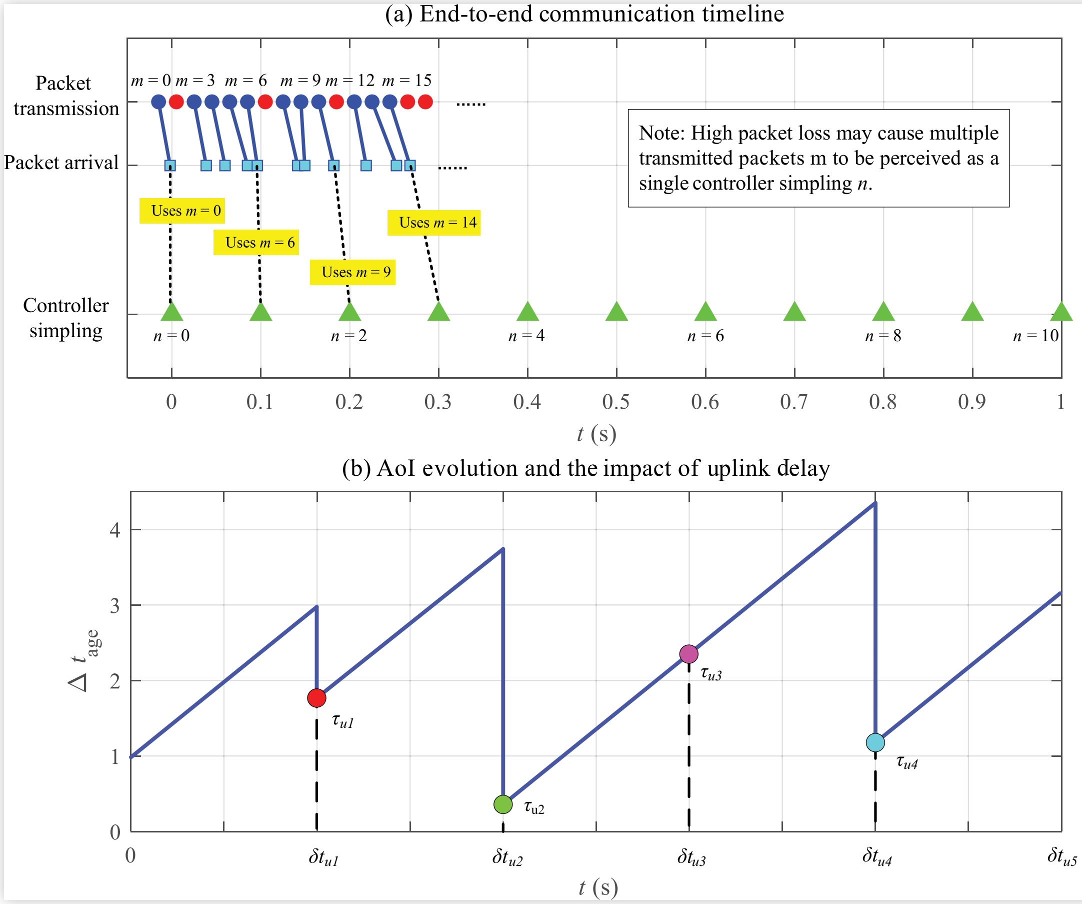

To simplify the following state matrix $\mathbf{A} \in \mathbb{R}^{2\times 2}$ and control matrix $\mathbf{B} \in \mathbb{R}^{2\times 1}$, each element is denoted by a_{ij} and b_{ij}, $(i, j = 1, 2)$, respectively.

Remark 1. *Regarding the choice of control strategy, the controller (6) is intentionally designed with a relatively simple state feedback structure. The primary objective of this work is to analytically investigate the fundamental impact of communication delays on closed-loop steering stability. A structurally simple controller allows the delay-induced effects, such as phase lag, damping reduction, and oscillatory instability, to be explicitly reflected in the system dynamics and stability conditions. In this case, we choose the simple state feedback control regime to investigate the delay-induced performance.*

2.4. Controller Design under Network-Induced Time-Varying Delays

In practical networked driving environments, communication delays are inherently time-varying and stochastic due to packet transmission, scheduling, and processing uncertainties. To capture these effects, the delay is modeled as a bounded time-varying function $\tau(t)$.

The control structure is retained, while the delayed state arguments are updated accordingly:

$$\delta_d(t) = -k_p\beta\big(t-\tau(t)\big) - k_d\gamma\big(t-\tau(t)\big) \tag{9}$$

More advanced control strategies, such as observer-based feedback or predictive compensation, are not considered in this study because they would introduce additional system dynamics and design parameters, which may obscure the intrinsic effects of communication delays that this work aims to reveal. It should be noted that the proposed stability analysis framework can be extended to more advanced controllers, which will be investigated in future work.

Substituting this control law into the vehicle dynamics yields the following closed-loop system with time-varying delay:

$$\dot{x}(t) = \mathrm{A}x(t) + \mathrm{BK}x\big(t-\tau(t)\big) \tag{10}$$

Compared with the constant delay case, the presence of $\tau(t)$ introduces additional challenges in stability analysis, as both the magnitude and variation rate of the delay may affect the system dynamics. These effects necessitate the use of $\mathcal{L}-\mathcal{K}$ functional–based techniques to derive delay-dependent stability conditions, which are addressed in the subsequent section.

3. Stability Analysis

In this section, we analyze the stability of steering control systems under both constant delay and network-induced time-varying delay. Stability in time delay systems is classified into delay-independent region, which ensures stability regardless of delay magnitude, and delay-dependent region, which is maintained within specific delay thresholds. This section develops stability criteria for both categories, offering a comprehensive framework to evaluate the impact of delays on system performance.

3.1. Stability Region under Constant Delay

With a constant time delay τ, the closed-loop characteristic equation is obtained by the exponential trial solution,

$$D(\lambda) = \det\left(\lambda \mathrm{I} - \mathrm{A} - \mathrm{BK}e^{-\lambda\tau}\right) = 0 \tag{11}$$

where λ is the characteristic exponent and $\mathbf{I} \in \mathbb{R}^{2\times 2}$ is the identity matrix. Using (8), (11) can be written explicitly as

$$D(\lambda) = \det\begin{bmatrix} \lambda - a_{11} - k_p b_1 e^{-\lambda\tau} & -a_{12} - k_d b_1 e^{-\lambda\tau} \\ -a_{21} - k_p b_2 e^{-\lambda\tau} & \lambda - a_{22} - k_d b_2 e^{-\lambda\tau} \end{bmatrix} \tag{12}$$

For a fixed delay τ, the $\mathcal{D}$-Subdivision method [33, 35] provides the stability boundary in the (k_p, k_d) plane. By repeating the procedure for different τ, one obtains a family of delay-dependent stability regions. As illustrated in Figure 4, these regions shrink as τ increases. However, $\mathcal{D}$-Subdivision is primarily a boundary-construction tool: it reveals the shrinkage trend but does not directly yield a rigorous delay-independent limit set nor the delay threshold at which such a limit is reached.

To obtain a conservative region that guarantees stability regardless of the delay magnitude, we compute a delay-independent stability set using $\mathcal{L}-\mathcal{K}$ functionals [45]. A classical $\mathcal{L}-\mathcal{K}$ functional for constant delay systems is

$$V(t) = x^T(t)\mathrm{P}x(t) + \int_{t-\tau}^{t} x^T(s)\mathrm{S}x(s)\,ds \tag{13}$$

where $\mathbf{P} = \mathbf{P}^T \succ 0$ and $\mathbf{S} = \mathbf{S}^T \succ 0$.

The resulting LMI conditions define a delay-independent stability region in the gain plane, shown as the light-blue set in Figure 4. This region serves as a robust baseline, but it is typically conservative and does not capture how stability depends on the actual delay value. Figure 4(a) and (b) show that increasing τ (e.g., from 0.1 s to 0.5 s) progressively reduces the $\mathcal{D}$-Subdivision stability region. For sufficiently large delays [Figure 4(c) and (d), e.g., $\tau \geq 1$ s], the delay-dependent region collapses to (or becomes close to) the delay-independent $\mathcal{L}-\mathcal{K}$ set. Therefore, the $\mathcal{L}-\mathcal{K}$ region can be interpreted as a conservative ultimate stability region for large delays, useful for robust controller tuning.

The term delay-independent stability region is a standard concept in time delay systems theory. It refers to a set of controller gains (k_p, k_d) for which the Lyapunov–Krasovskii functional satisfies $\dot{V} < 0$ without imposing any finite upper bound on the delay $\tau(t)$. In other words, for gains selected from this region, the closed-loop system is mathematically guaranteed to remain stable even if the delay grows arbitrarily large. A system can be Lyapunov-stable yet exhibit sluggish tracking or excessive oscillations when the delay becomes large. The delay-independent region should therefore be interpreted as a theoretical robustness certificate rather than as a guarantee of high-quality tracking under arbitrarily large delays. In practice, controller gains are selected from the delay-dependent region (which is larger and less conservative) based on the actual delay bounds measured from the communication network, so that both stability and satisfactory transient performance are ensured.

Remark 2. *The $\mathcal{D}$-Subdivision method provides accurate gain-dependent stability boundaries for each fixed delay, but it does not explicitly characterize the delay-independent limit set nor the delay threshold at which it is reached. In contrast, the $\mathcal{L}-\mathcal{K}$ approach yields an explicit delay-independent stability region, which can be used as a conservative reference for robust design.*

3.2. Stability Region for Network-Induced Time-Varying Delays

In practical systems, time delays are rarely constant and often vary over time. To better reflect real-world scenarios, our analysis extends to systems with network-induced time-varying delays. The stability-critical delay is determined by analyzing the system's network-induced time-varying dynamics to identify the control parameters

FIGURE 4 The $\mathcal{D}$-Subdivision and $\mathcal{L}-\mathcal{K}$ functionals stable region under various delays.

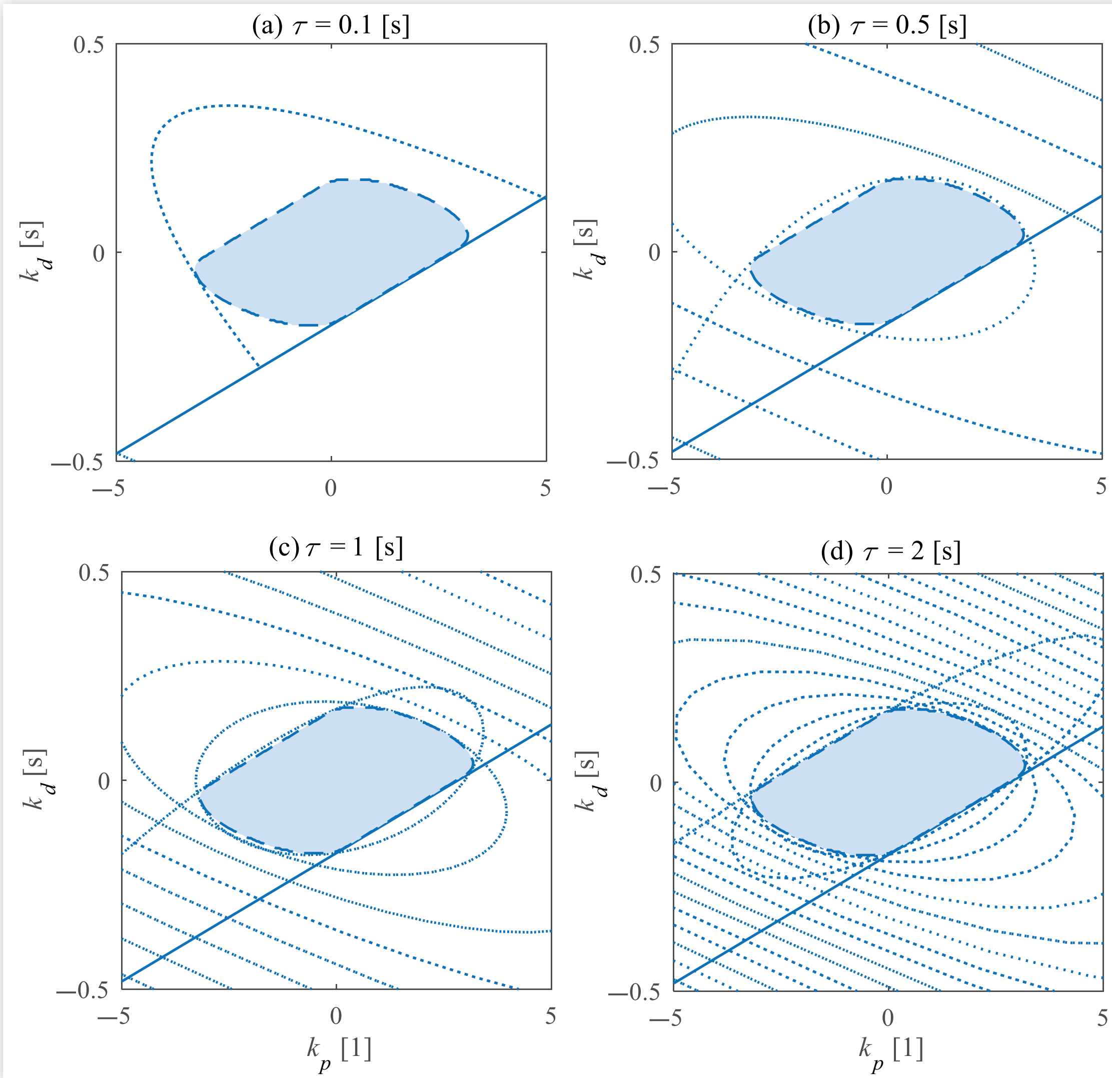

before instability. This approach ensures system stability within defined delay bounds. This section investigates the stability of the closed-loop system subject to time-varying delays. Different from conventional Jensen-based Lyapunov–Krasovskii approaches, a delay-partitioned functional formulated in terms of state increments is developed.

Consider the closed-loop system

$$\dot{x}(t) = Ax(t) + BKx(t - \tau(t)) \tag{14}$$

where the time-varying delay $\tau(t)$ satisfies

$$0 \le \tau(t) \le h, \quad \dot{\tau}(t) \le d < 1 \tag{15}$$

The delay $\tau(t)$ is continuously differentiable and satisfies (15) with known upper bounds $h > 0$ and $0 \le d < 1$.

For notational convenience, define the auxiliary vectors

$$v_1 = \frac{1}{h}\int_{t-h}^{t} x(s)\,ds, \quad v_2 = \frac{1}{h^2}\int_{t-h}^{t}\int_{s}^{t} x(u)\,du\,ds \tag{16}$$

and the augmented state

$$\eta(t) = \mathrm{col}\{x(t),\ x(t-h(t)),\ x(t-h),\ v_1,\ v_2\} \in \mathbb{R}^{5n} \tag{17}$$

Theorem 1. *For given scalars $h > 0$ and d, the system (14) subject to (15) is asymptotically stable if there exist matrices*

$$\begin{aligned} &\tilde{P} = \tilde{P}^\top \in \mathbb{R}^{3n\times 3n}, \quad \tilde{P} > 0 \\ &S = S^\top,\ Q = Q^\top,\ R_1 = R_1^\top,\ R_2 = R_2^\top \in \mathbb{R}^{n\times n} \\ &S > 0,\ Q > 0,\ R_1 > 0,\ R_2 > 0,\ X \in \mathbb{R}^{n\times n} \end{aligned} \tag{18}$$

such that the following LMIs hold:

$$\mathcal{R} \triangleq \begin{bmatrix} R_1 & X \\ X^\top & R_1 \end{bmatrix} \geq 0 \tag{19}$$

$$\Phi < 0 \tag{20}$$

where $\Phi \in \mathbb{S}^{5n}$ *is defined by*

$$\Phi = \mathcal{Z}^\top \tilde{P}\Lambda + \Lambda^\top \tilde{P}^\top \mathcal{Z} + \Sigma + h^2 \Pi^\top \left(R_1 + R_2\right)\Pi - \mathcal{D}^\top \mathcal{R}\mathcal{D}$$
$$-\sum_{k=0}^{2}\left(2k+1\right)\Omega_k^\top R_2\, \Omega_k \tag{21}$$

The matrices appearing in (21) are constructed from the selector matrices $e_i \in \mathbb{R}^{n\times 5n}(i = 1, \ldots, 5)$*, which extract the i-th n-dimensional block from* $\eta(t)$*, and are given as follows:*

$$\Pi = \left[A \;\; BK \;\; 0 \;\; 0 \;\; 0\right] \tag{22}$$

$$\mathcal{Z} = \begin{bmatrix} e_1 \\ e_4 \\ e_5 \end{bmatrix} \tag{23}$$

$$\Lambda = \begin{bmatrix} \Pi \\ \frac{1}{h}\left(e_1 - e_3\right) \\ \frac{1}{h}\left(e_1 - e_4\right) \end{bmatrix} \tag{24}$$

$$\Sigma = \mathrm{diag}\left\{S + Q,\; -\left(1-d\right)S,\; -Q,\; 0_n,\; 0_n\right\} \tag{25}$$

$$\mathcal{D} = \begin{bmatrix} e_1 - e_2 \\ e_2 - e_3 \end{bmatrix} \tag{26}$$

$$\Omega_0 = e_1 - e_3,\quad \Omega_1 = e_1 + e_3 - 2e_4,\quad \Omega_2 = e_1 - e_3 + 6e_4 - 12e_5 \tag{27}$$

The complete derivation process is deferred to Appendix A.

Remark 3. *The proposed criterion combines the reciprocally convex combination to handle the time-varying delay partition with the second-order Bessel–Legendre inequality to tighten the bound on the integral quadratic term over the full delay interval. Compared with criteria that rely solely on Jensen's inequality or the Wirtinger-based inequality, this combination exploits higher-order information of the state trajectory through* ν_1 *and* ν_2*, thereby reducing conservatism.*

Figure 5 shows the k_p–k_d stability regions obtained by three integral-inequality-based methods under constant delays $\tau \in \{0.10, 0.30\}$ s, with the delay-free boundary as an upper reference. At $\tau = 0.10$ s, all delay-dependent regions closely approximate the delay-free contour; however, the proposed Bessel–Legendre method ($N = 2$) already yields a larger feasible region than the Wirtinger and Jensen methods. As the delay increases to $\tau = 0.30$ s, the conservatism gap widens: the Jensen-based region shrinks significantly along the k_d axis, whereas the proposed method preserves a much larger admissible region. This demonstrates that the higher-order integral inequality reduces conservatism in the LKF-based stability criterion, with the improvement becoming more pronounced at larger delays.

Figure 6 further compares the three methods under time-varying delay $0 \leq \tau(t) \leq h$ with $\dot{\tau}\left(t\right) \leq 0.5$, where the constant delay proposed boundary is included for reference. Two key observations are noted. First, the relative advantage of the proposed method is further amplified

FIGURE 5 Stability region for constant delays.

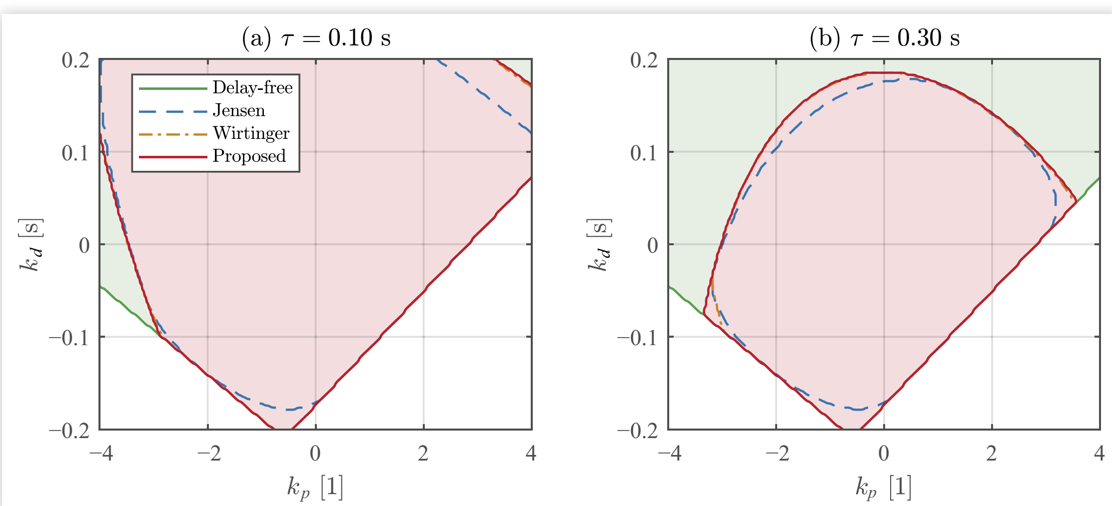

FIGURE 6 Stability region for time-varying delays.

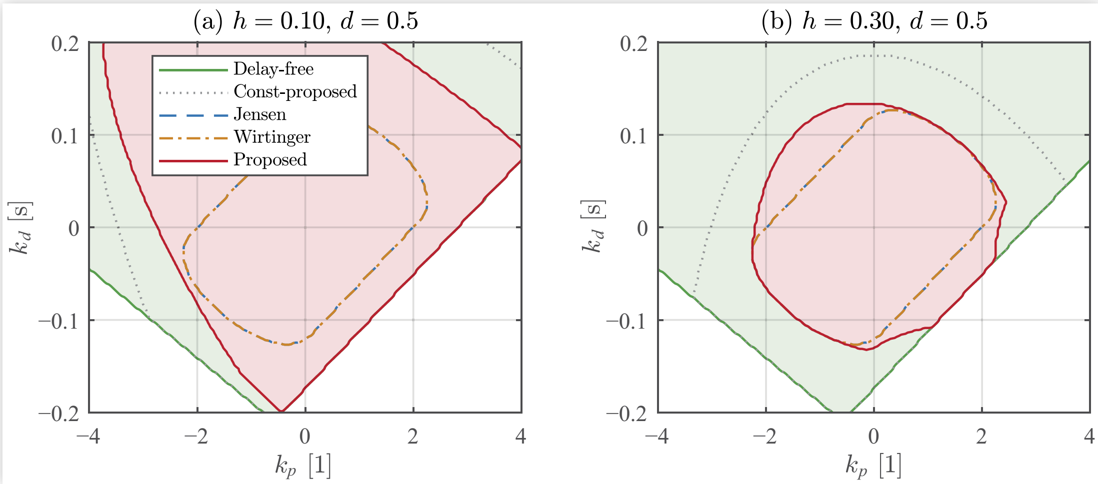

under time-varying delay, where it still guarantees a nontrivial two-dimensional design space. Second, this advantage is practically relevant, as communication-induced delays in networked or teleoperated driving systems are inherently stochastic and time-varying.

In summary, the proposed stability criterion consistently yields the least conservative k_p–k_d stability region among all methods, with more pronounced improvement under time-varying delays. This better reflects realistic communication delay characteristics and provides greater practical value for robust controller design.

Figure 7 characterizes the three-dimensional stability regions of the lateral control system under time-varying delays from two perspectives: a fixed delay bound h in (a) and a fixed delay rate d in (b). The LMI-derived boundaries form a distinctive dome-shaped structure that contracts monotonically as either h or d increases. In Figure 7(a), the stability region progressively shrinks as d increases, indicating that higher delay rates impose tighter constraints on the admissible gains. In Figure 7(b), the region undergoes rapid contraction as h increases from 0 to approximately 0.5 s; beyond this point, the cross-section changes only marginally, forming a near-vertical plateau. This observation implies that once the delay bound exceeds a certain threshold, the dominant constraint on stability shifts from the delay magnitude to the delay rate d. Since time delays in vehicle lateral control typically fall within 0.5 s, the proposed criterion provides the greatest discriminative capability within this practically relevant range. From a design perspective, Figure 7(b) shows that at a moderate delay rate (d = 0.5), stability can be maintained up to $h \approx 1.0$ s, whereas Figure 7(a) indicates that for h = 1 s, rapid delay variations require significantly more conservative gain tuning. These results

FIGURE 7 Stability region for network-induced time-varying delays.

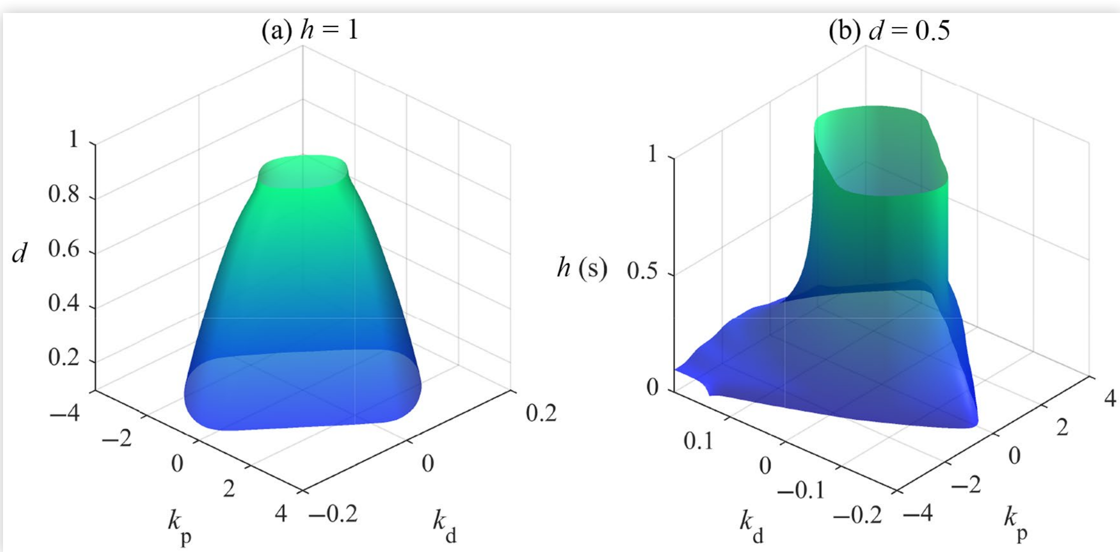

TABLE 2 Computational complexity comparison of the six LMI formulations (n = 2).

Method[1]	Decision variables	Max. LMI dimension	Avg. solve time (ms)
Jensen-C	9	$2n = 4$	44.2
Wirtinger-C	18	$3n = 6$	46.8
Proposed-C	30	$4n = 8$	49.5
Jensen-TV	12	$2n = 4$	47.1
Wirtinger-TV	24	$3n = 6$	51.3
Proposed-TV	37	$5n = 10$	55.8

[1] Time-varying and constant are denoted by TV and C.

confirm that time-varying delays impose stricter constraints than constant delays of the same magnitude, thereby underscoring the necessity of the proposed delay-aware synthesis framework.

Table 2 summarizes the computational complexity of the six LMI formulations, including the number of scalar decision variables, the maximum LMI block dimension, and the average per-point solution time measured on the test platform. The proposed method involves more decision variables and larger LMI blocks than the Jensen- and Wirtinger-based counterparts, due to the additional Legendre-projected augmented states introduced in the LKF. Specifically, the Proposed-TV formulation contains approximately four times as many decision variables and a maximum LMI block dimension that is 2.5 times larger than that of Jensen-C. Nevertheless, the actual solution time does not scale proportionally, because the computational bottleneck of interior-point semi-definite programming solvers is primarily determined by the largest LMI block size rather than the total number of variables. Consequently, Proposed-TV incurs less than a 1.3-fold increase in solution time relative to Jensen-C, while all six formulations remain on the order of tens of milliseconds per grid point.

These results confirm that the conservatism reduction demonstrated in Figures 5 and 7 is achieved with a modest and fully acceptable computational overhead. For the low-dimensional lateral vehicle dynamics considered in this study, the proposed method is well-suited for offline controller synthesis, as the entire k_p–k_d stability boundary can be swept within seconds on a standard desktop computer. This favorable complexity–conservatism trade-off further validates the practical merit of augmenting the LKF with higher-order Legendre-projected state integrals and leveraging the reciprocally convex combination lemma for delay rate-dependent stability analysis.

4. Numerical Simulations

4.1. Validation of Delay-Independent Stability Region

To validate the theoretical stability results, we simulate the vehicle system under various time delays. The simulations

FIGURE 8 The comparison between $\mathcal{D}$-Subdivision and $\mathcal{L}-\mathcal{K}$ functionals stable region.

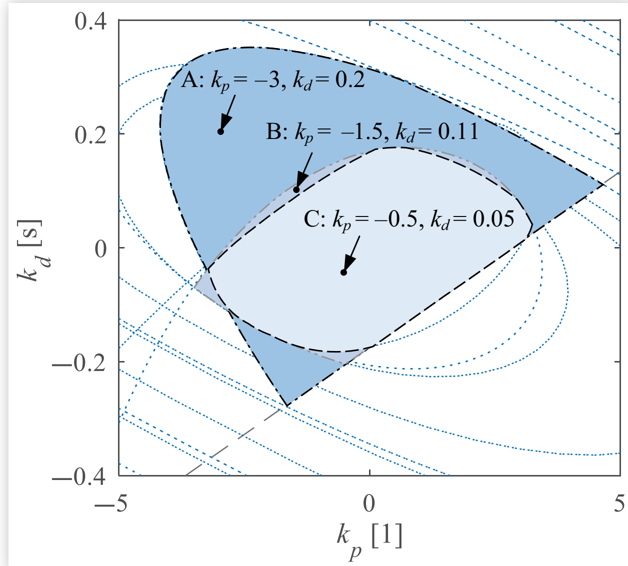

confirm that the system remains stable within the delay-independent region, as calculated using the $\mathcal{L}-\mathcal{K}$ functional method. To further analyze the system's dynamic behavior, the vehicle's yaw rate and sideslip angle responses are examined, demonstrating stable performance under different control parameters and time delay conditions.

To facilitate comparison and validate the stability regions, the $\mathcal{D}$-Subdivision stability diagrams for τ = 0.1 s, 0.5 s, and 1 s are integrated into Figure 8, with the shades of blue representing the stability regions, becoming progressively lighter as the delay increases. Control parameter Points A, B, and C (see Figure 8) are marked within their respective regions. A series of simulations (see Figures 9–11) validate these findings, confirming that the system remains stable under the delay-independent region.

Figures 9–11 describe the system's time-domain responses under varying time delays, highlighting the stability characteristics of different control parameter settings. Figures 9(a)–11(a) are the sideslip angle evolution, while Figures 9(b)–11(b) depict the corresponding yaw rate. At Point A (k_p = −3[1], k_d = 0.2[s]), regarding Figures 9, the system exhibits stability when the delay is 0.1 s. However, increasing the delay to 0.5 s and 1 s causes the system to become unstable, indicating that the control gains at this point are highly sensitive to delay variations. In contrast, at Point B (k_p = −1.4[1], k_d = 0.11[s]), with respect to Figure 10, the system remains stable for a delay of τ = 0.5 s, although the response exhibits minor oscillations before eventually converging. When the delay is further increased to τ = 1 s, the system transitions to instability. This suggests that while the control parameters at Point B exhibit some robustness to delays, their tolerance range is relatively limited. At Point C (k_p = −0.5[1], k_d = 0.05[s]), depicted in Figure 11, the system resides in the

FIGURE 9 Vehicle states under delay-independent region for Point A.

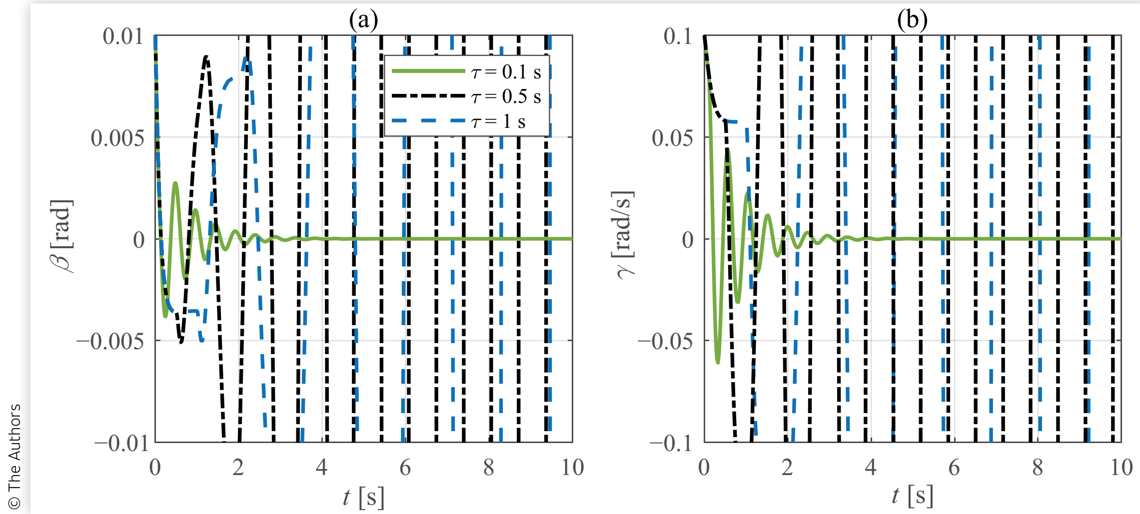

FIGURE 10 Vehicle states under delay-independent region for Point B.

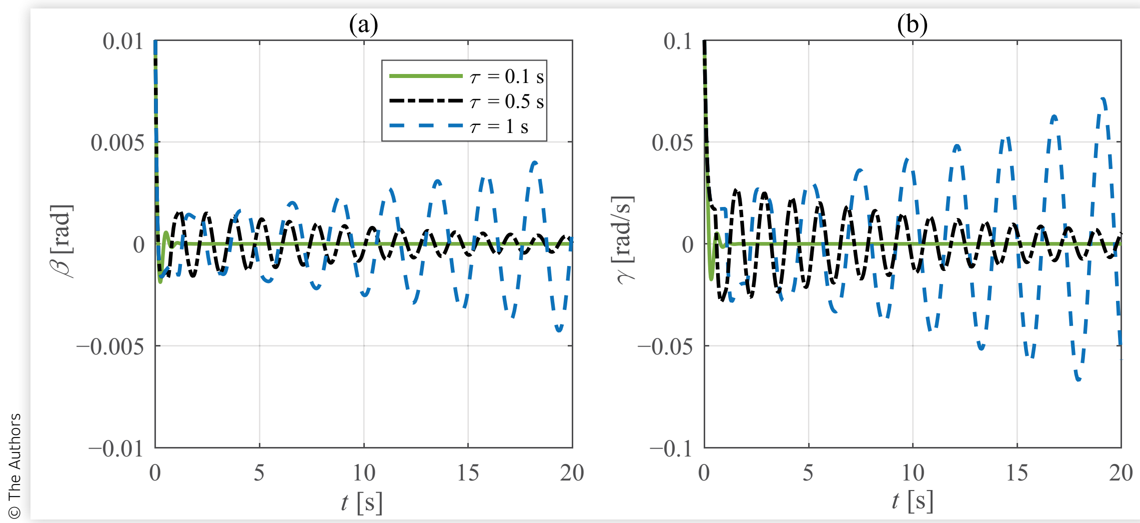

FIGURE 11 Vehicle states under delay-independent region for Point C.

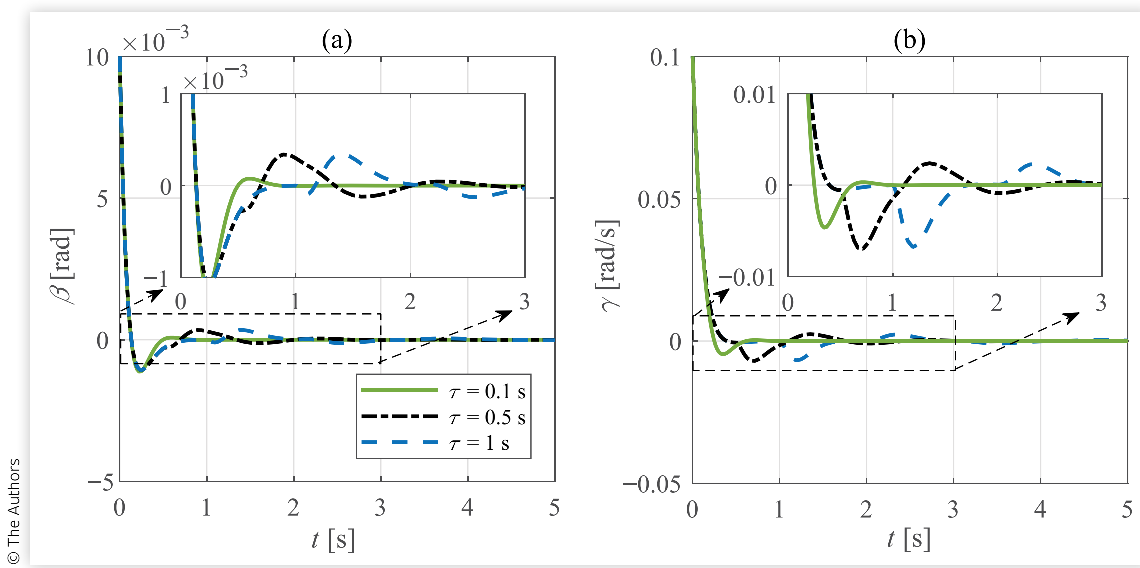

delay-independent stability region, maintaining stability and convergence regardless of the delay magnitude. This demonstrates a high degree of robustness, as the system's behavior remains unaffected by delays.

Remark 4. *These findings highlight the critical role of control parameter selection in ensuring stability under delayed feedback conditions. Parameters such as those at Point C are particularly robust, making them well-suited for applications involving significant delays, including vehicle dynamic control and autonomous driving systems.*

4.2. Validation of Stability Region of Network-Induced Time-Varying Delay

The controller performance is further evaluated under realistic time-varying delays arising from stochastic network effects induced by network variability and packet losses. Sampling intervals are set to $\delta t_{ul} = \delta t_{dl} = \delta t_a = 20$ ms, following [46], with a controller processing delay of $\delta t_p = 100$ ms and an actuation delay of $\tau_a = 100$ ms. The vehicle states are initialized at non-zero values ($\beta_0 = 0.01$ rad; $\gamma_0 = 0.2$ rad), representing a sudden lateral perturbation (e.g., a crosswind gust or a lane-change initiation). The uplink and downlink delays, τ_{ul} and τ_{dl}, follow the probabilistic model introduced in Subsection 2.2.

Two representative network scenarios are considered to emulate varying communication conditions between the vehicle and the controller [44, 47]:

- Case I (Low density & Low image quality): corresponds to a mild network disturbance with an average uplink delay of 9.9 ms, a downlink delay of 8.41 ms, and a packet drop ratio of 0.1%;
- Case II (High density & High image quality): represents a congested channel with a larger uplink delay of 24.14 ms, a similar downlink delay of 8.42 ms, and a severe packet loss of 82.4%.

TABLE 3 Network-induced delay statistics under Cases I and II.

Cases	Mean	Min	Max	Drop ratio
I	0.2839 s	0.2298 s	0.4293 s	0.1%
II	0.3732 s	0.2002 s	0.7321 s	82.4%

Critically, the peak values of 0.43 s and 0.73 s are not sustained delays. They arise from occasional packet loss events in the wireless channel: when one or more consecutive packets are dropped, the effective delay experienced by the control loop increases sharply at that particular sampling instant because the system must wait for the next successfully received packet. Under the zero-order hold strategy, the actuator continues to execute the last successfully received control command during these transient packet loss intervals; the vehicle is therefore not uncontrolled, but rather maintains its most recent steering input. Such instantaneous delay spikes occur only at isolated sampling instants and are immediately followed by a return to the nominal delay range once the next packet arrives successfully.

These two cases are designed to evaluate control robustness under both stable and degraded communication conditions [47]. It should be noted that the high packet loss scenario (82.4%) is considered as a worst-case condition to evaluate system robustness. In practical systems, packet loss is typically mitigated through retransmission or ZOH mechanisms, which result in bounded effective delays.

Figure 12(a) and (b) illustrate the temporal evolution of the delay and the corresponding probability density distributions, while the corresponding statistical characteristics are summarized in Table 3. In Case I, the E2E delay exhibits regular sawtooth-like fluctuations near the mean, reflecting stable transmission and negligible packet loss. In contrast, Case II shows irregular and widely varying delays caused by frequent uplink disruptions and packet drops, consistent with the trends reported in [32].

FIGURE 12 Statistical characteristics of network-induced delay.

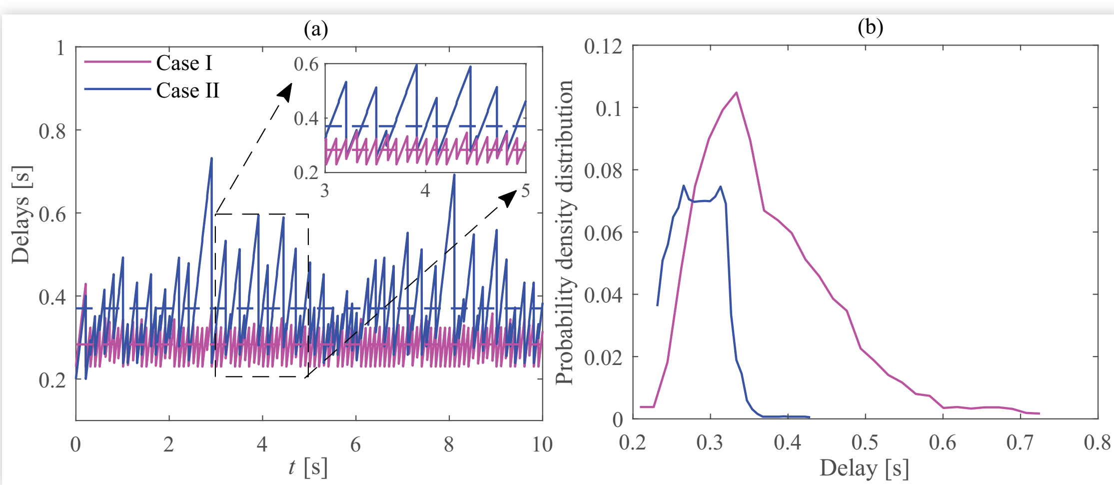

FIGURE 13 The sideslip angle β responses under Case I and Case II.

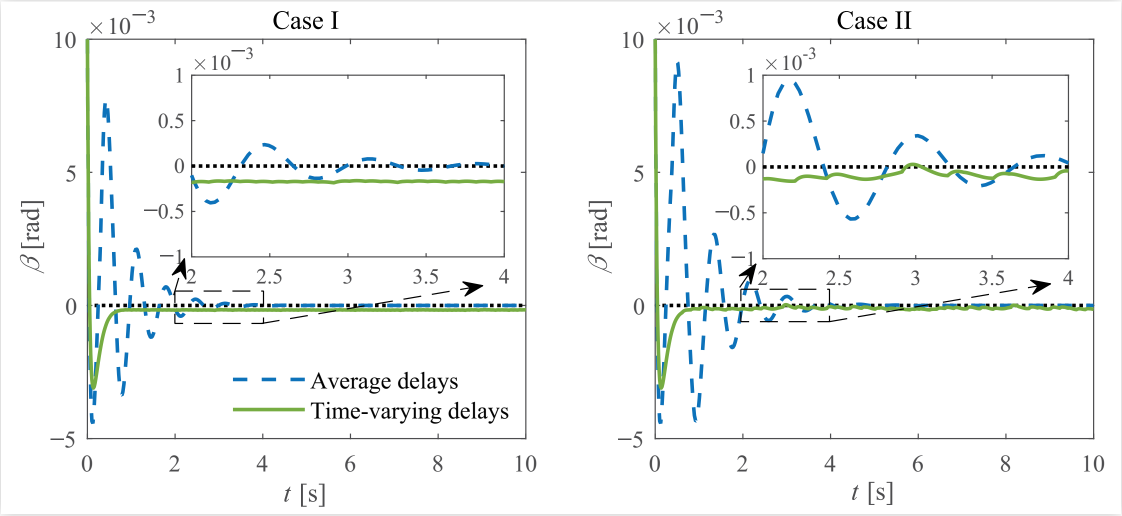

This comparison highlights the significant influence of network quality on the stability and responsiveness of automated steering control.

Figures 13–15 present the comparative tracking performance of the controller under network-induced time-varying delays (i.e., Case I and Case II). The results are analyzed in terms of sideslip angle, yaw rate, and steering angle responses. Transient performance analysis reveals that the time-varying delay model (solid green line) significantly outperforms the constant average-delay approach (dashed blue line) in both scenarios. For sideslip angle responses (see Figure 13), Case I shows a reduction in peak amplitude from approximately 0.15 rad to 0.09 rad, representing a 40% improvement in overshoot suppression. Case II demonstrates more pronounced differences, where the constant delay approach generates severe oscillations that persist well beyond the initial transient phase. The yaw rate responses (see Figure 14) exhibit similar trends, with initial oscillation peaks decreasing from 8×10^{-3} rad/s to approximately 5×10^{-3} rad/s under the time-varying delay model. *These improvements can be attributed to the accurate representation of real-time network conditions: when the controller accounts for instantaneous delay variations, it maintains appropriate control timing even as packet transmission intervals fluctuate, whereas the constant delay assumption introduces phase errors that accumulate into larger tracking deviations.*

Steady-state behavior highlights critical modeling limitations of the constant delay approach. As shown in the zoomed insets (t = 2 ~ 4 s) across all three state variables, the constant average-delay model exhibits persistent oscillations even after the initial transient has

FIGURE 14 The yaw rate γ responses under Case I and Case II.

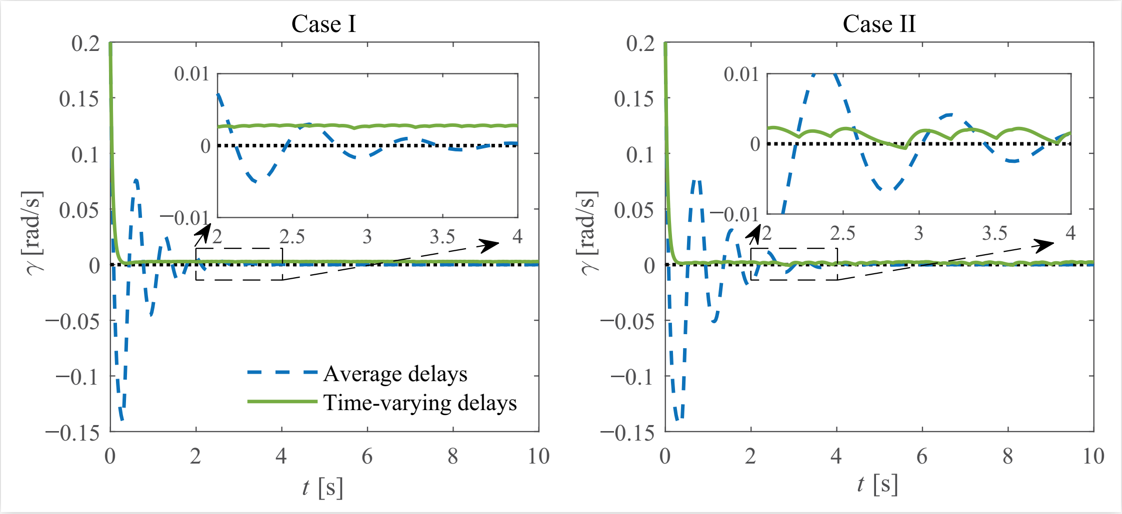

FIGURE 15 The steering angle δ under Case I and Case II.

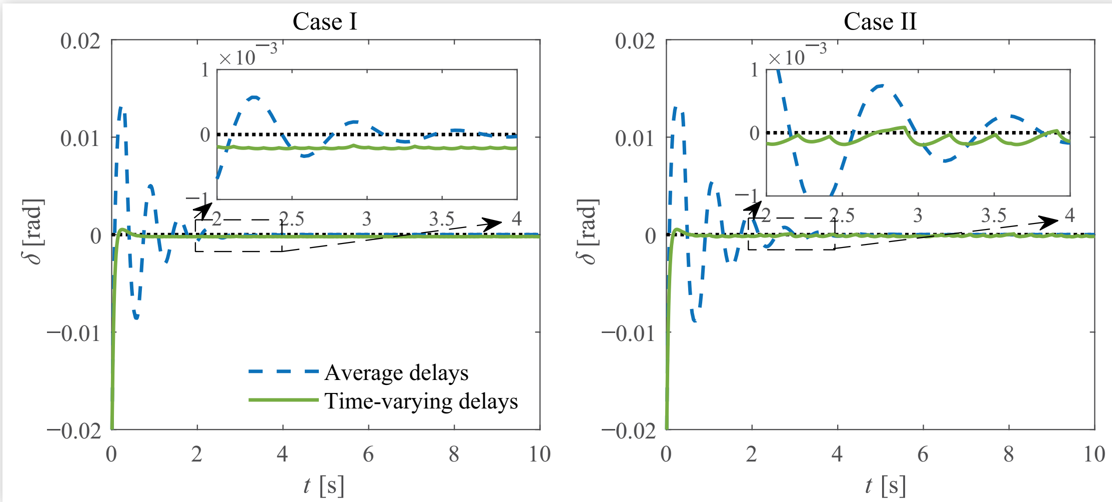

decayed. In Case II, the sideslip angle [Figure 13(b)] inset reveals sustained fluctuations, while the time-varying delay model converges to near-zero steady-state error. Similarly, the yaw rate [Figure 14(b)] inset demonstrates continued variations under constant delay assumptions, compared to the smooth convergence achieved by the time-varying delay model. This degradation is particularly evident when comparing Case I and Case II: the higher packet loss ratio in Case II corresponds to greater delay variability, making the constant delay approximation increasingly inaccurate. *The resulting modeling mismatch causes the closed-loop system to oscillate around the desired trajectory rather than achieving stable convergence, as the controller repeatedly over- and under-compensates based on outdated delay information.*

Control input characteristics (see Figure 15) further distinguish the two approaches. Although both methods generate similar initial control peaks (0.013 rad), the time-varying delay model produces smoother decay with significantly reduced oscillatory behavior. In Case I, both approaches converge to negligible control activity by t = 4 s, though the time-varying delay model settles slightly faster. However, in Case II, the distinction becomes pronounced: the constant delay model exhibits visible oscillations in the control input (amplitude $\pm 5 \times 10^{-3}$ rad in the inset), while the time-varying delay model produces steadier commands with minimal fluctuations ($\pm 0.2 \times 10^{-3}$ rad). These high-frequency control variations have important practical implications. For steer-by-wire actuators, oscillatory control inputs can cause excessive motor current fluctuations, leading to increased energy dissipation in power electronics and accelerated wear in mechanical transmission components. Additionally, such control chattering can transmit unwanted vibrations to the steering column, degrading passenger comfort and creating a less refined driving experience.

4.3. Performance Metric Definitions

For a generic state channel $\xi \in \{\beta, \gamma, \delta\}$ with reference command $\xi_{\text{ref}}(t)$, the root-mean-square error (RMSE) is defined as

$$\text{RMSE}_{\xi} = \sqrt{\frac{1}{T}\int_0^T \left[\xi(t) - \xi_{\text{ref}}(t)\right]^2 dt} \tag{28}$$

which measures the average tracking deviation over the entire simulation horizon. A smaller RMSE_{ξ} indicates higher tracking fidelity. The RMSE values for all three channels are depicted in Figure 16.

The p% settling time $T_{s,\xi}^{p\%}$ is defined as the smallest time instant after which the response remains within a $\pm p$% band of its steady-state value $\xi_{\infty} = \lim_{t\to\infty}\xi(t)$:

$$T_{s;\xi}^{p\%} = \inf\left\{t^* > 0 \,\middle|\, \left|\xi(t) - \xi_{\infty}\right| \le \frac{p}{100}\left|\xi_{\infty} - \xi(0)\right|,\ \forall t \ge t^*\right\} \tag{29}$$

A shorter settling time indicates a faster transient response. The 2% settling times for all channels are compared in Figure 17.

To evaluate the impact of delay modeling on closed-loop performance, the proposed controller is tested under both the average-delay and the time-varying-delay conditions in Cases I and II using identical gain structures. Two metrics are considered: RMSE and settling time. As shown in Figure 16, the controller under time-varying delay consistently achieves lower RMSE across all channels. In Case I, the RMSE of β, γ, and δ is

FIGURE 16 The RMES of β, γ, δ responses under Case I and Case II.

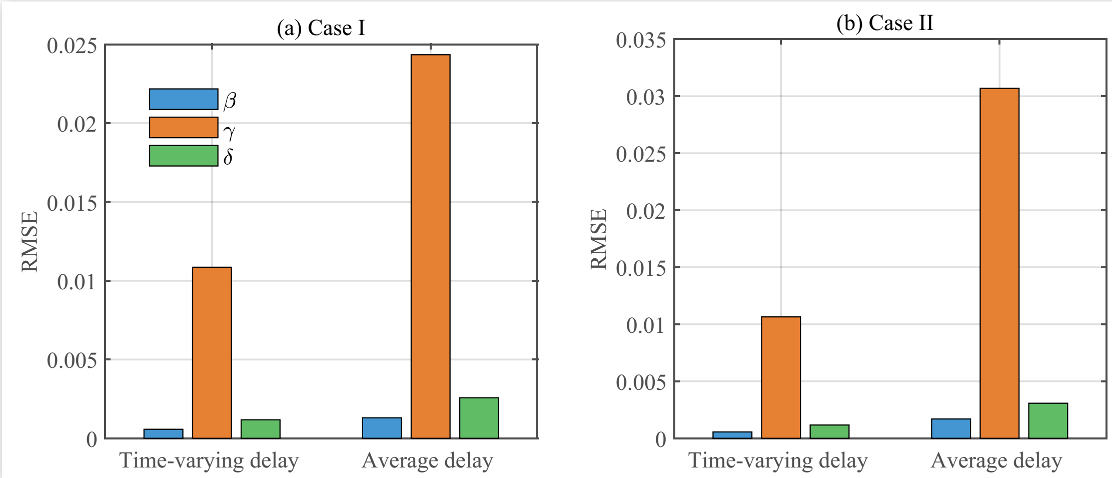

reduced by **56.0%**, **55.4%**, and **54.3%**, respectively, compared to the average-delay case. In Case II, the reductions increase to **67.1%**, **65.3%**, and **62.1%**, indicating improved accuracy due to delay variability. Settling time results (see Figure 17) further demonstrate this advantage. In Case I, the controller under time-varying delay achieves $T^{2\%}_{s,\beta} = 0.715$ s, $T^{2\%}_{s,\gamma} = 0.230$ s, and $T^{2\%}_{s,\delta} = 0.290$ s, whereas under average delay the corresponding values are 2.522 s, 2.329 s, and 2.296 s. In Case II, the settling time under average delay increases further, whereas the time-varying delay case remains nearly unchanged, demonstrating strong robustness.

Remark 5. *The comparative analysis reveals performance degradation at two levels. First, modeling accuracy matters critically: the constant delay approach deteriorates catastrophically in Case II, with oscillations increasing by* 120%, *indicating a near-loss of control authority, while the time-varying model maintains relative stability. Second, network quality sets fundamental limits: even with accurate delay modeling, Case II exhibits residual oscillations* ($\pm 0.2 \times 10^{-3}$ *rad in control input insets) absent in Case I. When* 82.4% *of packets are lost, the controller operates on severely outdated data regardless of modeling sophistication. These findings underscore that connected vehicle control requires both precise delay representation and reliable network infrastructure. While accurate modeling is necessary for acceptable performance, adequate network quality remains a prerequisite for safety-critical operation.*

While this study focuses on controlled network delays, real-world deployment of remote vehicle coordination systems faces additional challenges, including packet loss, jitter, bandwidth fluctuations, and cybersecurity threats such as denial-of-service and man-in-the-middle attacks. These factors are beyond the scope of the current study but warrant systematic investigation in future work to ensure the robustness, reliability, and safety of practical networked vehicle control systems.

FIGURE 17 The settling time of β, γ, δ responses under Case I and Case II.

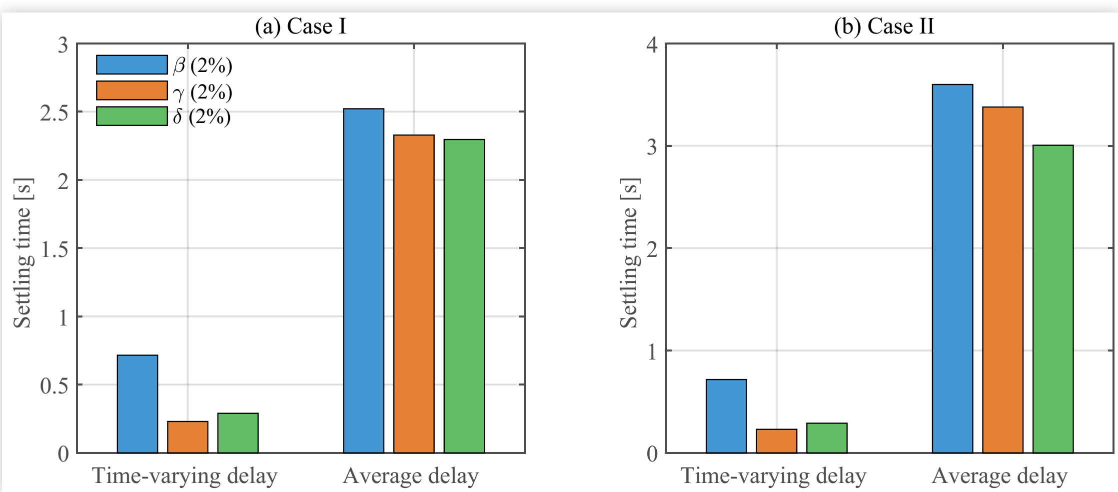

5. Conclusions

This study presents a cross-layer framework that integrates realistic V2N2V delay characterization with rigorous stability analysis of automated vehicle steering control under both constant and network-induced time-varying communication delays. The analytical, LMI-based, and simulation results consistently reveal how delay magnitude, delay variability, and packet loss jointly influence the closed-loop stability and performance of networked steering systems.

The constant delay analysis identifies a delay-independent stability region that guarantees closed-loop stability for all admissible delays. Outside this region, the critical delay threshold decreases with increasing control gains, thereby quantitatively characterizing the inherent gain–delay trade-off in steering control. For network-induced time-varying delays, LKF combined with refined integral inequalities yields delay-dependent LMI conditions that capture the joint influence of delay bounds and delay rate variations. The admissible stability region contracts with increasing delay magnitude or delay rate variability, while the derivative channel exhibits heightened sensitivity to these variations.

Simulation studies demonstrate that incorporating the measured time-varying V2N2V delay profile, rather than relying on a simple average-delay assumption, substantially improves closed-loop performance under identical gain structures. However, at high packet loss rates, the limited availability of state information leads to noticeable residual oscillations, indicating that the effectiveness of delay compensation strategies degrades as communication reliability deteriorates. These findings highlight that accurate delay modeling at the network layer translates directly into tangible control performance gains at the vehicle layer, thereby reinforcing the value of the cross-layer perspective adopted in this work. Future work will focus on gain adaptation and network-aware compensation strategies to further enhance robustness under severe communication constraints.

Declaration of Competing Interest

The authors declare that they have no known competing financial interests or personal relationships that could have appeared to influence the work reported in this paper.

Acknowledgements

The authors sincerely thank the coauthors, Jianwei Lu, Heng Wei, and Di Ao, reviewers, and the editor for their invaluable contributions and constructive feedback. This work is supported by the National Natural Science Foundation of China (Grant Nos. 52402477; 52472447); the Guangdong Basic and Applied Basic Research Foundation (Grant No. 2026A1515010257); the Special Funding for the Construction of the High-Level Academy of Agricultural Sciences (Grant No. NYQS202618).

Declaration of AI-Assisted Technologies

This manuscript was proofread using ChatGPT-5, an AI-powered language model developed by OpenAI. The tool was used to refine grammar, enhance clarity, and improve the readability of the text. All technical content, data interpretations, and conclusions were independently reviewed and verified by the authors to ensure accuracy and integrity. The use of ChatGPT-5 was solely for linguistic and stylistic improvements, with no influence on the scientific or analytical aspects of the manuscript. After using this tool/service, the authors reviewed and edited the content as needed and take full responsibility for the content of the publication.

Contact Information

Di Ao
Institute of Facility Agriculture, Guangdong Academy of Agricultural Sciences, Guangzhou, 510640, China
aodi@gdaas.cn

References

1. Hu, H., Tang, M., Chen, G., Gao, Z. et al., "Design of a Fault-Tolerant Control Algorithm for Four-Wheel Steering Vehicle Steering Locking Based on Dynamic Model Reconstruction," *SAE Int. J. Veh. Dyn., Stab., and NVH* 9, no. 4 (2025): 623-644, doi:https://doi.org/10.4271/10-09-04-0036.
2. Liang, J., Shen, C., Xia, X., Pi, D. et al., "Robust Game-Theory Control for All-Wheel Steering to Enhance Vehicle Handling Stability Performance," *IEEE Transactions on Systems, Man, and Cybernetics: Systems* 55, no. 12 (2025): 9230-9241, doi:https://doi.org/10.1109/TSMC.2025.3615943.
3. Lu, H., Wu, X., Zhao, S., Ren, Y. et al., "Going Beyond the Limit: Use the Unexploited Domain of Maneuverability to Negotiate Safe Vehicle Cornering," *Nonlinear Dynamics* 114, no. 5 (2026): 387, doi:https://doi.org/10.1007/s11071-026-12272-7.
4. Marumo, Y., Yokota, T., and Aoki, A., "Improving Stability and Lane-Keeping Performance for Multi-Articulated

Vehicles Using Vector Follower Control," *Vehicle System Dynamics* 58, no. 12 (2020): 1859-1872, doi:https://doi.org/10.1080/00423114.2019.1651877.

5. Fang, Z., Wang, J., Wang, Z., Chen, J. et al., "Human–Machine Shared Control for Path Following Considering Driver Fatigue Characteristics," *IEEE Transactions on Intelligent Transportation Systems* 25, no. 7 (2024): 7250-7264, doi:https://doi.org/10.1109/TITS.2023.3347439.
6. Li, J., Takacs, D., Lu, J., Voros, I. et al., "Exploring Optimal Feedback Delays of Lane-Keeping Controller," *Vehicle System Dynamics* (2025): 1-20, doi:https://doi.org/10.1080/00423114.2025.2532179.
7. Lu, Y., Zhong, J., Khoshnevisan, L., Sun, C. et al., "A Review on Vehicle Steer-by-Wire Control Systems," *Vehicle System Dynamics* (2025): 1-33, doi:https://doi.org/10.1080/00423114.2025.2589913.
8. Xue, Y., Wang, C., Ding, C., Yu, B. et al., "Observer-Based Event-Triggered Adaptive Platooning Control for Autonomous Vehicles with Motion Uncertainties," *Transportation Research Part C: Emerging Technologies* 159 (2024): 104462, doi:https://doi.org/10.1016/j.trc.2023.104462.
9. Yu, J., Jiang, F., Luo, Y., and Kong, W., "Improved Model-Free Adaptive Predictive Control-Based Cooperative Driving Control for Connected and Automated Vehicles Subject to Time-Varying Communication Delays and Packet Losses at Signal-Free Intersections," *IET Intelligent Transport Systems* 16, no. 10 (2022): 1427-1440, doi:https://doi.org/10.1049/itr2.12222.
10. Silva, E.A., Mozelli, L.A., Neto, A.A., and Souza, F.O., "Disturbance and Uncertainty Compensation Control for Heterogeneous Platoons under Network Delays," *Computers and Electrical Engineering* 123 (2025): 110066, doi:https://doi.org/10.1016/j.compeleceng.2025.110066.
11. Jang, J.Y., Ahn, S., and Kim, T.W., "Cloud-Based Information System for Automated Precast Concrete Transportation Planning," *Automation in Construction* 152 (2023): 104942, doi:https://doi.org/10.1016/j.autcon.2023.104942.
12. Liao, G., Fang, Z., Wang, J., Yin, G. et al., "A Hierarchical Shared Control Framework for Distributed Drive Electric Vehicles Considering Driving Ability and Energy Efficiency," *IEEE Transactions on Transportation Electrification* 12, no. 3 (2026): 4557-4570, doi:https://doi.org/10.1109/TTE.2026.3670946.
13. Zhang, J., Zhang, B., Zhang, N., Wang, C. et al., "A Novel Robust Event-Triggered Fault Tolerant Automatic Steering Control Approach of Autonomous Land Vehicles under In-Vehicle Network Delay," *International Journal of Robust and Nonlinear Control* 31, no. 7 (2021): 2436-2464, doi:https://doi.org/10.1002/rnc.5393.
14. Morawski, M. and Ignaciuk, P., "Reducing Impact of Network Induced Perturbations in Remote Control Systems," *Control Engineering Practice* 55 (2016): 127-138, doi:https://doi.org/10.1016/j.conengprac.2016.06.019.
15. Zhou, X., Ao, D., Zhang, J., Huang, J. et al., "A Bioinspired Structure-Based Adaptive Constraint-Following Control for Nonlinear Suspension Systems with Measurement Errors," *Green Energy and Intelligent Transportation* (2026): 100403, doi:https://doi.org/10.1016/j.geits.2026.100403.
16. Zhang, S.-W., Ma, L., Li, Q., and Wang, H., "Observer-Based Adaptive Path Tracking Control for Autonomous Ground Vehicle with Singularities and Time-Varying Delays," *Journal of Mechanical Science and Technology* 39, no. 3 (2025): 1443-1456, doi:https://doi.org/10.1007/s12206-025-0236-z.
17. Liang, J., Lu, Y., Wang, F., Feng, J. et al., "ETS-Based Human–Machine Robust Shared Control Design Considering the Network Delays," *IEEE Transactions on Automation Science and Engineering* 22 (2025): 17501-17511, doi:https://doi.org/10.1109/TASE.2024.3383094.
18. Hu, X., Zhang, Y., Hu, Y., Wang, Z. et al., "Time-Varying Gain-Scheduled Path-Tracking Controller with Delay Compensation (TGDC) for Autonomous Vehicles," *SAE Int. J. Veh. Dyn., Stab., and NVH* 9, no. 2 (2025): 209-227, doi:https://doi.org/10.4271/10-09-02-0012.
19. Asperti, M., Vignati, M., and Sabbioni, E., "Design of Electric Power Steering Control for Compensating the Torque Steer Effect Due to Torque Vectoring Control," *SAE Int. J. Veh. Dyn., Stab., and NVH* 9, no. 2 (2025): 177-193, doi:https://doi.org/10.4271/10-09-02-0010.
20. Zhang, X., Li, J., Zhou, J., Zhang, S. et al., "Vehicle-to-Everything Communication in Intelligent Connected Vehicles: A Survey and Taxonomy," *Automotive Innovation* 8, no. 1 (2025): 13-45, doi:https://doi.org/10.1007/s42154-024-00310-2.
21. Viadero-Monasterio, F., Nguyen, A.-T., Lauber, J., Boada, M.J.L. et al., "Event-Triggered Robust Path Tracking Control Considering Roll Stability under Network-Induced Delays for Autonomous Vehicles," *IEEE Transactions on Intelligent Transportation Systems* 24, no. 12 (2023): 14743-14756, doi:https://doi.org/10.1109/TITS.2023.3321415.
22. Voros, I., Orosz, G., and Takacs, D., "On the Global Dynamics of Path-Following Control of Automated Passenger Vehicles," *Nonlinear Dynamics* 111, no. 9 (2023): 8235-8252, doi:https://doi.org/10.1007/s11071-023-08284-2.
23. Cheng, S., Li, L., Chen, X., and Wu, J., "Model-Predictive-Control-Based Path Tracking Controller of Autonomous Vehicle Considering Parametric Uncertainties and Velocity-Varying," *IEEE Transactions on Industrial Electronics* 68, no. 9 (2020): 8698-8707, doi:https://doi.org/10.1109/TIE.2020.3009585.
24. Ao, D., Wong, P.K., and Huang, W., "Model Predictive Control Allocation Based on Adaptive Sliding Mode Control Strategy for Enhancing the Lateral Stability of Four-Wheel-Drive Electric Vehicles," *Proceedings of the Institution of Mechanical Engineers, Part D: Journal of Automobile Engineering* 238, no. 6 (2024): 1514-1534, doi:https://doi.org/10.1177/09544070221147327.
25. Wei, H., Lu, J., Shi, L., Lu, H. et al., "Modal Analysis and Dynamic Shimmy Behavior of Vehicle–Road System," *Journal of Vibration and Control* 29, no. 1-2 (2023): 387-399, doi:https://doi.org/10.1177/10775463211048266.
26. Lu, H., Lu, J., Wei, H., Shi, L. et al., "On the Non-Linear Dynamics of Vehicle Shimmy Coupled with Handling

Motions: Modelling, Bifurcation Analysis, and Validations," *Journal of Vibration and Control* 29, no. 15-16 (2023): 3435-3450, doi:https://doi.org/10.1177/10775463221096258.

27. Rahmanei, H., Aliabadi, A., Ghaffari, A., and Azadi, S., "Lyapunov-Based Control System Design for Trajectory Tracking in Electrical Autonomous Vehicles with In-Wheel Motors," *Journal of the Franklin Institute* 361, no. 6 (2024): 106736, doi:https://doi.org/10.1016/j.jfranklin.2024.106736.
28. Ding, X., Du, Z., Gao, M., and Wang, H., "Assessment of Takeover Safety in Human–Machine Co-Driving on Grassland Highways: Coupling Effects of Non-Driving-Related Tasks and Takeover Scenarios," *Transportation Research Part F: Traffic Psychology and Behaviour* 114 (2025): 376-408, doi:https://doi.org/10.1016/j.trf.2025.06.003.
29. Ghorai, P., Eskandarian, A., and Kim, Y.-K., "Study the Effect of Communication Delay for Perception and Collision Avoidance in Cooperative Autonomous Driving," in *ASME International Mechanical Engineering Congress and Exposition*, Vol. 84553, 2020, V07BT07A015, American Society of Mechanical Engineers, (Virtual, Online) https://doi.org/10.1115/IMECE2020-24008.
30. Xu, X., Liu, Z., Wang, F., Xie, J. et al., "Trajectory Tracking Control Based on the Dual-Motor Autonomous Steering System with Time-Varying Network-Induced Time Delay," *Control Engineering Practice* 116 (2021): 104915, doi:https://doi.org/10.1016/j.conengprac.2021.104915.
31. Sun, Y., Xu, J., Chen, C., and Hu, W., "Reinforcement Learning-Based Optimal Tracking Control for Levitation System of Maglev Vehicle with Input Time Delay," *IEEE Transactions on Instrumentation and Measurement* 71 (2022): 1-13, doi:https://doi.org/10.1109/TIM.2022.3142059.
32. Bartfai, A., Voros, I., and Takacs, D., "Stability Analysis of a Digital Hierarchical Steering Controller of Autonomous Vehicles with Multiple Time Delays," *Journal of Vibration and Control* 30, no. 1-2 (2024): 330-341, doi:https://doi.org/10.1177/10775463221146624.
33. Lu, H., Stepan, G., Lu, J., and Takacs, D., "Dynamics of Vehicle Stability Control Subjected to Feedback Delay," *European Journal of Mechanics-A/Solids* 96 (2022): 104678, doi:https://doi.org/10.1016/j.euromechsol.2022.104678.
34. Wu, G., "Impact of Positioning Uncertainty on Connected and Automated Vehicle Applications," *SAE Int. J. CAV* 6, no. 2 (2022): 155-168, doi:https://doi.org/10.4271/12-06-02-0010.
35. Voros, I. and Takacs, D., "Lane-Keeping Control of Automated Vehicles with Feedback Delay: Nonlinear Analysis and Laboratory Experiments," *European Journal of Mechanics-A/Solids* 93 (2022): 104509, doi:https://doi.org/10.1016/j.euromechsol.2022.104509.
36. Song, Y., Li, Z.-Y., and Zhou, B., "Stability Analysis of Linear Neutral Delay Systems with Two Delays via Augmented Lyapunov–Krasovskii Functionals," *IEEE Transactions on Circuits and Systems I: Regular Papers* 70, no. 1 (2022): 460-471, doi:https://doi.org/10.1109/TCSI.2022.3216576.
37. Zeng, H.-B., Zhou, S.-J., Zhang, X.-M., and Wang, W., "Delay-Dependent Stability Analysis of Load Frequency Control Systems with Electric Vehicles," *IEEE Transactions on Cybernetics* 52, no. 12 (2022): 13645-13653, doi:https://doi.org/10.1109/TCYB.2022.3140463.
38. Hernandez-Gonzalez, O., Targui, B., Valencia-Palomo, G., and Guerrero-Sánchez, M.E., "Robust Cascade Observer for a Disturbance Unmanned Aerial Vehicle Carrying a Load under Multiple Time-Varying Delays and Uncertainties," *International Journal of Systems Science* 55, no. 5 (2024): 1056-1072, doi:https://doi.org/10.1080/00207721.2023.2301496.
39. Dinçmen, E., "Neural Network Steering Control Algorithm for Autonomous Ground Vehicles Having Signal Time Delay," *Proceedings of the Institution of Mechanical Engineers, Part I: Journal of Systems and Control Engineering* 238, no. 4 (2024): 720-736, doi:https://doi.org/10.1177/09596518231199208.
40. Jin, L., He, Y., Zhang, C.-K., Jiang, L. et al., "Delay-Dependent Stability of Load Frequency Control with Adjustable Computation Accuracy and Complexity," *Control Engineering Practice* 135 (2023): 105518, doi:https://doi.org/10.1016/j.conengprac.2023.105518.
41. Qin, W.B. and Orosz, G., "Experimental Validation of String Stability for Connected Vehicles Subject to Information Delay," *IEEE Transactions on Control Systems Technology* 28, no. 4 (2019): 1203-1217, doi:https://doi.org/10.1109/TCST.2019.2900609.
42. Javani, A., Zorgui, M., and Wang, Z., "Age of Information for Multiple-Source Multiple-Server Networks," *IEEE Transactions on Networking* 33, no. 1 (2025): 17-34, doi:https://doi.org/10.1109/TNET.2024.3474052.
43. Boada, M.J.L., Boada, B.L., and Zhang, H., "Event-Triggering H∞-Based Observer Combined with NN for Simultaneous Estimation of Vehicle Sideslip and Roll Angles with Network-Induced Delays," *Nonlinear Dynamics* 103, no. 3 (2021): 2733-2752, doi:https://doi.org/10.1007/s11071-021-06269-7.
44. Ji, X.A., Avedisov, S.S., Khan, M.I., Lucas-Estan, M.C. et al., "Fundamental Rules of Teleoperated Driving with Network Latency on Curvy Roads," in *2024 IEEE Intelligent Vehicles Symposium (IV)*, Jeju Island, Republic of Korea, 2024, 1841-1846, IEEE, doi:https://doi.org/10.1109/IV55156.2024.10588495.
45. Li, W., Xie, Y., Li, Y., Geng, K. et al., "Robust Lateral Motion Control of Distributed Drive Vehicle Considering Long Input Delays," *International Journal of Robust and Nonlinear Control* 33, no. 5 (2023): 3185-3209, doi:https://doi.org/10.1002/rnc.6561.
46. Coll-Perales, B., Lucas-Estañ, M.C., Shimizu, T., Gozalvez, J. et al., "End-to-End v2x Latency Modeling and Analysis in 5G Networks," *IEEE Transactions on Vehicular Technology* 72, no. 4 (2022): 5094-5109, doi:https://doi.org/10.1109/TVT.2022.3224614.
47. Ji, X.A., Avedisov, S.S., Khan, M.I., Vörös, I. et al., "On the Effects of Latency in Teleoperated Driving: Stability and Performance Analysis," *Vehicle System Dynamics* (2025): 1-23, doi:https://doi.org/10.1080/00423114.2025.2537409.

Appendix: Proof of Theorem 1

Define the auxiliary vectors

$$\nu_1(t) = \frac{1}{h}\int_{t-h}^{t} x(s)ds, \quad \nu_2(t) = \frac{1}{h^2}\int_{t-h}^{t}\int_{s}^{t} x(u)du\,ds \tag{A.1}$$

and $\zeta(t) = \mathrm{col}\{x(t), \nu_1(t), \nu_2(t)\} \in \mathbb{R}^{3n}$.

Choose the Lyapunov–Krasovskii functional $V(x_t) = V_1 + V_2 + V_3 + V_4$ with

$$V_1 = \zeta^\top(t)\tilde{P}\zeta(t) \tag{A.2}$$

$$V_2 = \int_{t-h(t)}^{t} x^\top S x\,ds \tag{A.3}$$

$$V_3 = \int_{t-h}^{t} x^\top Q x\,ds \tag{A.4}$$

$$V_4 = h\int_{-h}^{0}\int_{t+\theta}^{t} \dot{x}^\top(R_1 + R_2)\dot{x}\,ds\,d\theta \tag{A.5}$$

Direct differentiation gives $\dot{\nu}_1 = \frac{1}{h}\left[x(t) - x(t-h)\right]$, $\dot{\nu}_2 = \frac{1}{h}\left[x(t) - \nu_1\right]$. Introducing the augmented vector $\eta(t) = \mathrm{col}\{x(t), x(t-h(t)), x(t-h), \nu_1, \nu_2\}$ and the selector matrices $e_i (i = 1, \ldots, 5)$, we can write $\zeta = \mathcal{Z}\eta$ and $\dot{\zeta} = \Lambda\eta$ with $\mathcal{Z}$, Λ as in (23)–(24). Hence,

$$\dot{V}_1 = \eta^\top\left(\mathcal{Z}^\top\tilde{P}\Lambda + \Lambda^\top\tilde{P}^\top\mathcal{Z}\right)\eta \tag{A.6}$$

By the Leibniz rule and $\dot{h}(t) \le d$,

$$\dot{V}_2 + \dot{V}_3 \le \eta^\top\Sigma\eta, \quad \Sigma = diag\left\{S + Q, -(1-d)S, -Q, 0_n, 0_n\right\} \tag{A.7}$$

Differentiating (A.5) yields

$$\dot{V}_4 = h^2\dot{x}^\top(R_1 + R_2)\dot{x} - h\int_{t-h}^{t}\dot{x}^\top(R_1 + R_2)\dot{x}\,ds \tag{A.8}$$

The first term equals $\eta^\top[h^2\Pi^\top(R_1 + R_2)\Pi]\eta$ via $\dot{x} = \Pi\eta$. For the integral term, write it as $\mathcal{I}_1 + \mathcal{I}_2$ by splitting $R_1 + R_2$.

Split the integration at $t-h(t)$ and apply Jensen's inequality on each sub-interval. Setting $\alpha = h(t)/h$, we obtain

$$\mathcal{I}_1 \le -\frac{1}{\alpha}d_1^\top R_1 d_1 - \frac{1}{1-\alpha}d_2^\top R_1 d_2 \tag{A.9}$$

with $d_1 = x(t) - x(t - h(t))$, $d_2 = x(t - h(t)) - x(t - h)$.

By the reciprocally convex combination lemma, if $\mathcal{R} = \begin{bmatrix} R_1 & X \\ X^\top & R_1 \end{bmatrix} \ge 0$, the right-hand side is further bounded by

$$\mathcal{I}_1 \le -\eta^\top\mathcal{D}^\top\mathcal{R}\mathcal{D}\eta, \ \mathcal{D} = \begin{bmatrix} e_1 - e_2 \\ e_2 - e_3 \end{bmatrix} \tag{A.10}$$

Apply the Bessel–Legendre inequality of order $N = 2$ on $[t-h, t]$ to get

$$\mathcal{I}_2 \le -\sum_{k=0}^{2}(2k+1)\eta^\top\Omega_k^\top R_2\Omega_k\eta \tag{A.11}$$

where Ω_0, Ω_1, Ω_2 are given in (27), corresponding to the projections of $\dot{x}$ onto the first three shifted Legendre polynomials.

Summing (A.6)–(A.11) gives $\dot{V} \le \eta^\top\Phi\eta$ with Φ as in (21). The condition $\Phi < 0$ ensures $\dot{V} < 0$ for all $\eta \ne 0$, which by the Lyapunov–Krasovskii theorem implies asymptotic stability. □